Fatigue crack detection in pipes with multiple mode nonlinear guided waves

Ruiqi Guan[1], Ye Lu[1,*], Kai Wang[2], Zhongqing Su[2]

[1]*Department of Civil Engineering*

Monash University

Clayton, VIC 3800, Australia

[2] *Department of Mechanical Engineering*

The Hong Kong Polytechnic University

Kowloon, Hong Kong SAR

[*] To whom all correspondence should be addressed

Email: *ye.lu@monash.edu* (Dr Ye LU) Fax: +61-3-9905-4944

Abstract

This study elaborates fundamental differences in fatigue crack detection using nonlinear guided waves between plate and pipe structures and provides an effective approach for analysing nonlinearity in pipe structures. For this purpose, guided wave propagation and interaction with microcrack in a pipe structure, which introduced a contact acoustic nonlinearity (CAN), was analysed through a finite element analysis in which the material nonlinearity was also included. To validate the simulation results, experimental testing was performed using piezoelectric transducers to generate guided waves in a specimen with a fatigue crack. Both methods revealed that the second harmonic wave generated by the breathing behaviour of the microcrack in a pipe had multiple wave modes, unlike the plate scenario using nonlinear guided waves. Therefore, a proper index which considered all the generated wave modes due to the microcrack was developed to quantify the nonlinearity, facilitating the identification of microscale damage and further assessment of the severity of the damage in pipe structures.

Introduction

With their advantages of long propagation distance and high sensitivity, guided waves are effective for pipeline inspection [1]. Different types of wave modes propagate in pipe-like structures, and the interaction between these modes and damage can be used to detect the location and size of the damage. Much research has been directed towards detecting cracks with different orientations, including radial depth extent [2], circumferential extent [3, 4] and axial extent [5-7] of the crack, corrosion pits [8, 9] and cracks in pipe welds [10]. In practice, longitudinal modes and torsional modes are commonly selected, having the advantages of non-dispersion over a wide frequency range and ease of excitation. However, guided wave based methods using linear wave characteristics are limited by the excited wavelength being capable of detecting only gross damage. In some circumstances, microscale damage such as initiation of fatigue cracks, early stage corrosion and material degradation need to be detected with high sensitivity techniques. Guided wave based methods using nonlinear wave characteristics are therefore preferred for these cases. These techniques focus on the nonlinear distortion of excited waves caused by the damage, including higher harmonic generation, mixed frequency responses, subharmonic generation, etc.

In this respect, theoretical analyses and numerical simulations in terms of material nonlinearity and contact acoustic nonlinearity (CAN) have shown great progress in plate structures. De Lima [11] ascertained two conditions, phase velocity matching and non-zero power flux, which need to be satisfied for the generation of the cumulative second harmonic using perturbation method and modal analysis. These conditions were further analysed by Müller et al. [12] with analytical asymptotic solutions to Lamb waves in plates with material nonlinearity. For the theory of CAN, Richardson [13] provided a model containing two semi-infinite elastic materials with intimate contact without traction forces on the interface to understand this type of nonlinearity. Rudenko and Vu [14] considered a model with traction forces between contact

surfaces. A bilinear stiffness model [15] with changeable stiffness under different phases of a wave was also an attractive analytical model. Among numerical methods for simulating material nonlinearity or CAN, the local interaction simulation approach (LISA) [16, 17], the finite element method (FEM) [18, 19] and the time-domain spectral finite element method (SFE) [20] are representative methods. Many experimental studies have also been conducted on plate structures, focusing on material nonlinearity [21, 22] and CAN induced by fatigue crack [23-29].

Due to the curvature of a pipe structure, the wave properties are more complex than in a plate. Theoretical and numerical analyses of higher harmonic generation have been conducted in nonlinear waveguides with arbitrary cross-section [30], in weakly nonlinear cylinders [31-33] and from plates to large radius pipes [34]. Simulation has shown that the cumulative second harmonic generation with longitudinal, torsional or flexural mode excitation was also observed in pipe structures when those two conditions, phase velocity matching and non-zero power flux, as in a plate structure were satisfied. Moreover, the simulation method of material nonlinearity in plate structures can also be applied to pipe counterparts. Experiments concerning material nonlinearities in pipes [35, 36] have also confirmed the phenomenon of cumulative second harmonic generation with longitudinal or circumferential wave excitation.

In terms of CAN, however, limited studies are found in pipe structures, where the presence of flexural wave modes makes interpretation of the second harmonic wave more difficult. The objective of this paper is to simulate material nonlinearity and “breathing” crack in an aluminium pipe as well as to carry out experimental testing for exploration of the second harmonic generation caused mainly by CAN.

This paper is organised as follows. Proper mode selection based on the dispersion curve is first introduced for prediction of the wave characteristics and understanding of numerical and experimental studies, where the methodology adopted in the simulation is also demonstrated.

Then, investigations including both numerical analysis and experiment testing are presented, followed by relevant results and comparisons with cases of plate structures. An appropriate nonlinear index suitable for pipe structures is provided after analysing the simulation and experimental results. The conclusion suggests future relevant work.

Mode selection

To select an appropriate wave mode for second harmonic generation, the dispersion curve of an aluminium pipe with 30 mm outer diameter and 4 mm wall thickness was plotted, as in Figure 1. To avoid the cumulative effect induced by material nonlinearity and highlight the second harmonic generated by CAN, wave mode L(0, 2) at 300 kHz was selected, which would be converted to L(0, 3) at 600 kHz but with a different group velocity as shown in Figure 1. Therefore, the cumulative effect of material nonlinearity would be minimised due to the group velocity difference. Meanwhile, from the dispersion curve, it could be observed that the lower order flexural wave modes, F(n, 2), had group velocities close to the longitudinal wave L(0, 2). In this case, more than one wave mode would be generated from the same group, unless a specific arrangement of wave excitation was designed. For convenience, a notation from Rose [37] was adopted in the subsequent study, in which L(n, m) was defined as a longitudinal mode group, including axisymmetric modes L(0, m) and non-axisymmetric modes F(n, m). The integer *m* is the circumferential order of a mode and the integer *n* denotes the group order of a mode. In this study, therefore, the fundamental waves were a group of waves L(n, 2) consisting of longitudinal mode L(0, 2) and flexural modes F(n, 2) (n=1,2,3…).

Simulation model

Different numerical techniques are usually used to investigate the interaction between guided waves and damage, such as spectral element method [38] and finite element method [39] , also, similar numerical methods used to simulate different microcrack models were discussed in [40].

In this study, a 3D model simulated by Abaqus/Explicit with a seam crack was utilised to analyse the propagation of longitudinal and flexural wave modes and the nonlinearity caused by both the material and the "breathing" crack.

An aluminium pipe 4 mm thick, 30 mm outer diameter and 1 m long was modelled. A through-thickness notch 8 mm long and 2 mm wide was prepared in the middle of the pipe for fatigue crack initiation. The central excitation frequency was selected as 300 kHz and a 6-cycle tone burst signal was excited. The excitation signal was applied as a pointed load at four edges of the transducer along the direction of the axis of the pipe. As only one actuator was used in the model, L(n, 2) consisting of both longitudinal mode L(0, 2) and flexural modes F(n, 2) at the selected frequency were generated. Two monitoring points were located in front of and behind the notch for receiving transmitted and reflected signals respectively. The arrangement of the actuator, notch and monitoring points is shown in Figure 2.

Three-dimensional eight-node brick elements (C3D8R) were utilised and the maximum element size in the model was 1 mm, which was roughly 18 elements per wavelength for L(0, 2) mode and 9 elements per wavelength for L(0, 3) mode. A time step of 5e-8 s based on the equation $\Delta t \leq L_{max}/c_g$ [41] was selected for stability of calculation, where L_{max} is the maximum element size in this model and c_g is the fastest group velocity among all wave modes.

To introduce the material nonlinearity which exists homogeneously in the simulation model, third order elastic constants [30] were considered for material properties and then imported into the model with a user subroutine VUMAT file [18]. The material properties are listed in Table 1. To model the "breathing" crack in the model, the seam crack definition was used on each surface of the crack, as illustrated in Figure 3, to enable the breathing behaviour when waves interacted with the crack. Meanwhile, a surface-to-surface contact interaction and associated properties were defined on the crack interface to achieve the modelling of CAN [18]. The crack

was through-thickness and 1 mm long in the circumferential direction, located at both tips of the notch.

Experimental validation

Experimental testing was performed for validation of the simulation results. An aluminium pipe with the same material properties and dimensions as in the simulation model was used in the experiment. To induce a microcrack, a steel frame was designed to hold the pipe and was combined with the fatigue machine. The pipe was therefore under three-point bending with a cyclic load in the middle, as in Figure 4. The cyclic load ranged from 0.2 kN to 2 kN with a 5 Hz load frequency. Rectangular piezoelectric transducers 5 mm×10 mm acting as both actuator and receivers were attached on the pipe in a line with the same locations as in the simulation model (in Figure 2). A signal generating and collecting system (see Figure 5) including Ritec RAM-5000 SNAP and an Agilent digital oscilloscope was used to generate and receive the signals. The system also contained a high-power low-pass filter which could suppress harmonics higher than 300 kHz from the source before the signal was input to the transducer.

A 6-cycle tone burst signal at a central frequency of 300 kHz was applied on the actuator and the reflected and transmitted signals were monitored by sensors until the second harmonic wave appeared in received signals when fatigue cycles reached 22000. All the received signals were averaged 1024 times with the sampling frequency of 200 MHz before recording. Also, the load from the fatigue machine was removed during signal collection to prevent any influence of external load on the "breathing" behaviour of the fatigue crack. To ensure that the nonlinearity monitored was induced by the opening and closing behaviour of the fatigue crack, application of the cyclic load was continued until the nonlinearity in the signal disappeared at about 42000 fatigue cycles, which indicated that the crack had developed to macro size. In the final stage, the pipe side with the fatigue crack was turned 180° to face downwards and then a static load

was applied upwards to the middle of the bottom of the pipe to close the crack, to observe whether the “breathing” behaviour still existed in the crack.

Results

Signal processing method

A similar signal processing method was used for the numerical and experimental analyses. After each signal was received, a 180° out-of-phase signal was input to the pipe again at the same location, followed by the same signal collection procedure. These two received signals were then superimposed to reduce the fundamental component contribution and enhance the second harmonic [42]. Subsequently, the short-time Fourier transform (STFT) was performed on each of the combined signals, and the component slices at double frequency were extracted and converted back to the time domain using the inverse fast Fourier transform [18]. Meanwhile, the STFT was also applied on the original signals before they were superimposed with the 180° out-of-phase signals and the slices at fundamental frequency were also extracted. Finally, signals of fundamental and double frequencies in the time domain were obtained and interpreted. The processing procedure is flowcharted in Figure 6.

Results from numerical simulation

For the transmitted signal, the signal received directly from simulation is shown in Figure 7. Due to the single transducer excitation, more than one wave packet appears in the received signal. The arrival time of the first wave packet is 83 μs, which is consistent with the theoretical velocity of L(0, 2) from the dispersion curve, followed by flexural wave modes. Signals after processing for the case with material nonlinearity only are shown in , which are in the time domain at fundamental frequency and at double frequency. It is obvious that the second harmonic wave arrives at the same time as the fundamental wave. The average amplitude level at double frequency is about 0.01% of that at 300 kHz.

Figure 9 shows the case with a seam crack, in which the signal at fundamental frequency displays no great difference from that with material nonlinearity only, while the second harmonic wave arrives later than the fundamental one, since the group velocity of L(0, 3) at double frequency was slower than that of L(0, 2) at fundamental frequency, reflecting the fact that the nonlinearity was induced by the microcrack. There are also multiple waves generated at double frequency before the arrival time of L(0, 1), which contains longitudinal mode L(0, 3) and flexural modes from the same group F(n, 3). The average amplitude of the second harmonic wave is approximately 1.3% of the fundamental wave. This phenomenon differs from that reported from a similar experiment in plate-like structures [25], where only one wave packet was generated at double frequency. The present results may be caused by multiple input wave modes, and with more than one mode generated at double frequency when a single wave mode was input.

For the reflected signal (Figure 10), the first arriving wave packet is L(n, 2) directly from the actuator, followed by reflected L(n, 2) from the notch and the direct L(n, 1). In the case with material nonlinearity at double frequency, the waves arrive at almost the same time as the fundamental wave, and the average amplitude level at double frequency is also around 0.04% of that at fundamental frequency. As for the model with the seam crack in Figure 11, the first arriving wave at double frequency is at 72 μs, which indicates the arrival of L(0, 3). There are also multiple wave packets before the arrival of L(0, 1) at 107 μs, with the average amplitude approximately 1.2% of the fundamental wave, which is much higher than the amplitude caused by material nonlinearity.

Results from experiment

The received transmitted signal from experiments is shown in Figure 12. The arrival time of the first wave packet is around 86 μs, which is very close to the velocity in simulation. There were also similar multiple wave packets within the period of interest from 86 μs to 126 μs,

which contains L(0, 2) and F(n, 2) modes as a group of L(n, 2). The shape of the received wave was slightly different from that obtained in the simulation results, due to the unavoidable differences between simulation and experiments, e.g. the efficiency of the transducer and certain flexural modes that were not generated appropriately. For the case without the introduction of fatigue crack in the pipe, some material nonlinearities existed and the signals after processing are plotted in Figure 13(a). From the figure, it can be seen that the second harmonic wave arrives at approximately the same time as the fundamental wave. However, the average amplitude of the second harmonic wave is about 0.8% of that in fundamental signal, which is much higher than in the corresponding simulation results. This difference is acceptable since ideally in practice the material is not homogeneous and there are also inherent nonlinear sources from the equipment and environment.

During the fatigue test, signal collection was stopped at 22000 fatigue cycles when an obvious increase in the second harmonic wave was observed in the signals. Comparison of the signals before and after fatigue testing is shown in Figure 14(a). As in the simulation results, the second harmonic wave (red line) arrives later than the benchmark signal in experiments and more than one generated wave packet is higher than the wave packets caused by material nonlinearity. The average amplitude level is above 2% of the signal at the fundamental frequency. To confirm that the results from the experiment is repeatable, another specimen with the same configuration was also studied, and the result of the transmitted signals is shown in Figure 14(b), where the average amplitude of second harmonic wave in benchmark signal is about 0.9% of that in the fundamental signal and the average amplitude of the second harmonic wave in damage case is about 1.8% of the signal at the fundamental frequency, similar to the results from the first specimen.

For the reflected signals (Figure 15), the received signal also contains direct wave L(n, 2), reflected L(n, 2) and direct L(n, 1), and the velocities of these wave packets are approximately

the same as those in the simulation results. The signal at double frequency shows that the first second harmonic wave arrived at 58 μs when there was only material nonlinearity and at 78 μs for the case of fatigue crack, which is close to the theoretical group velocity of L(0, 3) mode. Compared with the transmitted signal, the multi-mode second harmonic waves were not that apparent due to the short distance from the sensor to the micro crack, where the different wave modes have not been separated completely.

To confirm that the nonlinearity in the experiments was caused by the opening and closing behaviour of the fatigue crack under tension and the compression phase of guided waves, the pipe side with the crack was faced downwards for the first specimen after the nonlinearity was minimised to noise level in the collected signal. Then a static load at 100 N was applied upwards in an attempt to close the crack. The transmitted signals before and after applying the static load were recorded and processed with the same procedure as before, as illustrated in Figure 16. In the time period of interest, during which the second harmonic wave packet is expected to arrive, there is an obvious difference between the signals before and after applying the static load. The blue line shows that at the end of the fatigue test, the nonlinearity decreases to the noise level and the amplitude of second harmonic wave is much lower than that seen in Figure 14. In the red line, however, which represents the case where the static load was applied to close the crack, the amplitude of wave packets increases significantly at 97 μs, although it is still lower than that shown in Figure 14. Thus it was confirmed that the nonlinearity shown in Figure 14 and Figure 15 was caused by the fatigue crack. By the end of fatigue testing, however, the crack was too large to close entirely although its tip still evidenced breathing behaviour, which made a marginal contribution to the nonlinearity when the static load was applied.

Discussion

Compared to pipe structures, plate structures feature relatively simple dispersion curves, where fewer wave modes co-exist at a given frequency. Results from a previous study [43] of fatigue

crack detection using nonlinear guided waves in an aluminium plate are briefly introduced here to clarify the differences. The aluminium plate was 300 mm×450 mm and 3.18 mm thick, with a rivet hole in the middle for fatigue crack initiation. The excitation was a 15.5-cycle Hanning-windowed sinusoidal tone burst at the frequency of 1130 kHz and the fundamental wave was selected as S1. Circular PZTs were used as actuator and receiver respectively and only transmitted signals were considered. Details of the sensors and crack locations can be found in [43]. The simulation method of the seam crack was the same as that in the pipe model, and material nonlinearity was also introduced in the plate model.

From the simulation results shown in Figure 17, with one actuator excitation, a single wave mode S1 arrives at t_1 at fundamental frequency in the time domain and there is no great difference compared with the benchmark. At the double frequency, for the benchmark case there are already some nonlinearities from the material itself, similar to the pipe model case. In the case with fatigue crack, however, there is only one mode S2 at time t_2, which was induced by the damage. In contrast, in the case of pipe structures also with one actuator excitation, more than one wave mode was induced by the fatigue crack at double frequency, with close group velocities. The reason may be attributed to the fact that the group velocities of different wave modes, such as the antisymmetric mode and symmetric mode in plate structures, are distinct from each other and can be separated easily after a certain propagation distance. Therefore, the second harmonic wave from plate structures is generally simple with only one mode induced, whereas there would be multiple wave modes in pipe structures.

When nonlinearity in a plate structure is measured, a nonlinear parameter β is usually used, which is the ratio of the peak value of the amplitude of the second harmonic wave to the square of the peak value of the amplitude of the fundamental wave. However, when more than one wave packet presents at both fundamental and double frequencies, calculation of this parameter could not be carried out precisely and a new parameter is required to measure the nonlinearity.

In this circumstance, a parameter considering all generated wave packets was used, which was the envelope of the second harmonic wave within a time period divided by the envelope of the fundamental wave. The time window for the transmitted signal was selected from the arrival time of the first wave packet to the theoretical arrival time of wave mode L(0, 1), as shown in Figure 18. Therefore, the new nonlinear index was calculated by

$$Nonlinear\ index = \frac{Area\ 2}{Area\ 1} \quad (1)$$

Following equation (1), the nonlinear indices were calculated. The trend line in Figure 19 illustrates the nonlinear indices under the different conditions considered in this study for the pipe in experimental testing, i.e. (1) before fatigue testing as benchmark, (2) after 22000 cycles, (3) at the end of fatigue testing, and (4) with a static load. From the figure, it can be observed that the nonlinearity for both specimens shows the same trend. In detail, the index clearly increases at 22000 cycles compared with the benchmark and then drops to a level similar to that at the beginning after about 42000 cycles. It is understood that the difference in the index values for both specimens is mainly attributable to the unavoidable difference in test setting and installation conditions of transducers. With the application of a static load which closes part of the crack, the nonlinearity increases again but it is still much lower than that at 22000 cycles, indicating that the crack has developed into an open crack and only its tip had breathing behaviour under the static load.

Conclusions

This study provided comprehensive analyses of guided wave propagation and interaction with microcrack in a pipe structure through numerical and experimental approaches. Third order elastic constant and a seam crack were considered in the simulation model for material nonlinearity and CAN respectively. Piezoelectric transducers working with a nonlinear signal collecting system were adopted in the experimental testing for wave nonlinearity acquisition.

Both modelling and experimental results showed the nonlinearity caused by a “breathing” crack, and observation of multiple second harmonic waves was different from the results from a previous study in a plate structure. A new nonlinear index was proposed to measure the nonlinearity in pipe structures, which can be used to quantify microcrack severity for its propagation.

The phenomenon of multiple wave modes may be due to the influence of flexural waves in pipe structures, a proposition which will be verified by analytical studies in future work. Further study considering the quantitative assessment of the fatigue crack in pipes and the influence of other factors such as the sensor distance from the microcrack will be conducted as well.

References

[1] R. Guan, Y. Lu, W. Duan, and X. Wang, "Guided waves for damage identification in pipeline structures: A review," *Structural Control and Health Monitoring,* vol. 24, pp. e2007-e2007-17, 2017.

[2] D. N. Alleyne and P. Cawley, "The effect of discontinuities on the long-range propagation of Lamb waves in pipes," *Proceedings of the Institution of Mechanical Engineers, Part E: Journal of Process Mechanical Engineering,* vol. 210, pp. 217-226, 1996.

[3] D. N. Alleyne, M. J. S. Lowe, and P. Cawley, "The reflection of guided waves from circumferential notches in pipes," *Applied Mechanics,* vol. 65, pp. 635-641, 1998.

[4] H. S. Bai, A. H., N. Popplewell, and S. K. Datta, "Scattering of guided waves by circumferential cracks in composite cylinders," *International Journal of Solids and Structures,* vol. 39, pp. 4583–4603, 2002.

[5] P. W. Tse and X. Wang, "Semi-quantitative analysis of defect in pipelines through the use of technique of ultrasonic guided waves," *Key Engineering Materials,* vol. 413-414, pp. 109-116, 2009.

[6] P. W. Tse and X. Wang, "Characterization of pipeline defect in guided-waves based inspection through matching pursuit with the optimized dictionary," *NDT & E International,* vol. 54, pp. 171-182, 2013.

[7] X. Wang, P. W. Tse, and A. Dordjevich, "Evaluation of pipeline defect's characteristic axial length via model-based parameter estimation in ultrasonic guided wave-based inspection," *Measurement Science and Technology,* vol. 22, pp. 025701-025701-13, 2010.

[8] A. Demma, P. Cawley, M. Lowe, A. G. Roosenbrand, and B. Pavlakovic, "The reflection of guided waves from notches in pipes: a guide for interpreting corrosion measurements," *NDT & E International,* vol. 37, pp. 167-180, 2004.

[9] P. W. Tse and X. Wang, "Corrosion identification of gas pipe risers in buildings using advanced ultrasonic guided waves," in *Proceedings of the 7th World Congress on Engineering Asset Management (WCEAM 2012)*, ed: Springer International Publishing, 2015, pp. 583-592.

[10] M. J. S. Lowe, D. N. Alleyne, and P. Cawley, "The mode conversion of a guided wave by a part-circumferential notch in a pipe," *Journal of Applied Mechanics,* vol. 65, pp. 649-656, 1998.

[11] W. J. N. De Lima and M. F. Hamilton, "Finite-amplitude waves in isotropic elastic plates," *Journal of Sound and Vibration,* vol. 265, pp. 819-839, 2003.

[12] M. F. Müller, J.-Y. Kim, J. Qu, and L. J. Jacobs, "Characteristics of second harmonic generation of Lamb waves in nonlinear elastic plates," *The Journal of the Acoustical Society of America,* vol. 127, pp. 2141-2152, 2010.

[13] J. M. Richardson, "Harmonic generation at an unbonded interface—I. Planar interface between semi-infinite elastic media," *International Journal of Engineering Science,* vol. 17, pp. 73-85, 1979.

[14] O. V. Rudenko and C. A. Vu, "Nonlinear acoustic properties of a rough surface contact and acoustodiagnostics of a roughness height distribution," *Acoustic Physics,* vol. 40, pp. 593-596, 1994.

[15] I. Y. Solodov, N. Krohn, and G. Busse, "CAN: an example of nonclassical acoustic nonlinearity in solids," *Ultrasonics,* vol. 40, pp. 621-625, 2002.

[16] Y. Shen and C. E. S. Cesnik, "Local interaction simulation approach for efficient modeling of linear and nonlinear ultrasonic guided wave active sensing of complex structures," *Journal of Nondestructive Evaluation, Diagnostics and Prognostics of Engineering Systems,* vol. 1, pp. 011008-011008-9, 2017.

[17] Y. Shen and C. E. Cesnik, "Modeling of nonlinear interactions between guided waves and fatigue cracks using local interaction simulation approach," *Ultrasonics,* vol. 74, pp. 106-123, 2017.

[18] M. Hong, Z. Su, Q. Wang, L. Cheng, and X. Qing, "Modeling nonlinearities of ultrasonic waves for fatigue damage characterization: Theory, simulation, and experimental validation," *Ultrasonics,* vol. 54, pp. 770-778, 2014.

[19] Y. Liu, C. J. Lissenden, and J. L. Rose, "Cumulative second harmonics in weakly nonlinear plates and shells," in *SPIE Smart Structures and Materials+ Nondestructive Evaluation and Health Monitoring*, 2013, pp. 86950S-86950S-12.

[20] S. He and C. T. Ng, "Modelling and analysis of nonlinear guided waves interaction at a breathing crack using time-domain spectral finite element method," *Smart Materials and Structures,* vol. 26, p. 085002, 2017.

[21] C. Bermes, J.-Y. Kim, J. Qu, and L. J. Jacobs, "Experimental characterization of material nonlinearity using Lamb waves," *Applied Physics Letters,* vol. 90, pp. 021901-021901-3, 2007.

[22] K. H. Matlack, J.-Y. Kim, L. J. Jacobs, and J. Qu, "Experimental characterization of efficient second harmonic generation of Lamb wave modes in a nonlinear elastic isotropic plate," *Journal of Applied Physics,* vol. 109, pp. 014905-014905-5, 2011.

[23] C. Pruell, J.-Y. Kim, J. Qu, and L. J. Jacobs, "Evaluation of fatigue damage using nonlinear guided waves," *Smart Materials and Structures,* vol. 18, pp. 035003-035003-7, 2009.

[24] M. Deng and J. Pei, "Assessment of accumulated fatigue damage in solid plates using nonlinear Lamb wave approach," *Applied Physics Letters,* vol. 90, pp. 121902-121902-3, 2007.

[25] Y. Wang, R. Guan, and Y. Lu, "Nonlinear Lamb waves for fatigue damage identification in FRP-reinforced steel plates," *Ultrasonics,* vol. 80, pp. 87-95, 2017.

[26] J. Cheng, J. N. Potter, A. J. Croxford, and B. W. Drinkwater, "Monitoring fatigue crack growth using nonlinear ultrasonic phased array imaging," *Smart Materials and Structures,* vol. 26, p. 055006, 2017.

[27] Y. Yang, C.-T. Ng, A. Kotousov, H. Sohn, and H. J. Lim, "Second harmonic generation at fatigue cracks by low-frequency Lamb waves: Experimental and numerical studies," *Mechanical Systems and Signal Processing,* vol. 99, pp. 760-773, 2018.

[28] H. Lim and H. Sohn, "Necessary conditions for nonlinear ultrasonic modulation generation given a localized fatigue crack in a plate-like structure," *Materials,* vol. 10, p. 248, 2017.

[29] Y. Yang, C.-T. Ng, and A. Kotousov, "Influence of crack opening and incident wave angle on second harmonic generation of Lamb waves," *Smart Materials and Structures,* vol. 27, p. 055013, 2018.

[30] W. J. De Lima and M. F. Hamilton, "Finite amplitude waves in isotropic elastic waveguides with arbitrary constant cross-sectional area," *Wave Motion,* vol. 41, pp. 1-11, 2005.

[31] Y. Liu, C. J. Lissenden, and J. L. Rose, "Higher order interaction of elastic waves in weakly nonlinear hollow circular cylinders. I. Analytical foundation," *Journal of Applied Physics,* vol. 115, pp. 214901-214901-11, 2014.

[32] Y. Liu, E. Khajeh, C. J. Lissenden, and J. L. Rose, "Higher order interaction of elastic waves in weakly nonlinear hollow circular cylinders. II. Physical interpretation and numerical results," *Journal of Applied Physics,* vol. 115, pp. 214902-214902-10, 2014.

[33] Y. Liu, E. Khajeh, C. J. Lissenden, and J. L. Rose, "Interaction of torsional and longitudinal guided waves in weakly nonlinear circular cylinders," *The Journal of the Acoustical Society of America,* vol. 133, pp. 2541-2553, 2013.

[34] V. K. Chillara and C. J. Lissenden, "Analysis of second harmonic guided waves in pipes using a large-radius asymptotic approximation for axis-symmetric longitudinal modes," *Ultrasonics,* vol. 53, pp. 862-869, 2013.

[35] M. Deng, G. Gao, and M. Li, "Experimental observation of cumulative second-harmonic generation of circumferential guided wave propagation in a circular tube," *Chinese Physics Letters,* vol. 32, pp. 124305-124305-4, 2015.

[36] W. Li and Y. Cho, "Thermal fatigue damage assessment in an isotropic pipe using nonlinear ultrasonic guided waves," *Experimental Mechanics,* vol. 54, pp. 1309-1318, 2014.

[37] J. L. Rose, *Ultrasonic guided waves in solid media*. New York: Cambridge University Press, 2014.

[38] Y. Wang and H. Hao, "Modelling of guided wave propagation with spectral element: application in structural engineering," *Applied Mechanics and Materials,* vol. 553, pp. 687-692, 2014.

[39] L. Moreau, A. Velichko, and P. D. Wilcox, "Accurate finite element modelling of guided wave scattering from irregular defects," *NDT & E International,* vol. 45, pp. 46-54, 2012.

[40] D. Broda, W. J. Staszewski, A. Martowicz, T. Uhl, and V. Silberschmidt, "Modelling of nonlinear crack–wave interactions for damage detection based on ultrasound—a review," *Journal of Sound and Vibration,* vol. 333, pp. 1097-1118, 2014.

[41] O. Diligent, T. Grahn, A. Boström, P. Cawley, and M. J. S. Lowe, "The low-frequency reflection and scattering of the S0 Lamb mode from a circular through-thickness hole in a plate: Finite Element, analytical and experimental studies," *The Journal of the Acoustical Society of America,* vol. 112, pp. 2589-2601, 2002.

[42] J.-Y. Kim, L. J. Jacobs, J. Qu, and J. W. Littles, "Experimental characterization of fatigue damage in a nickel-base superalloy using nonlinear ultrasonic waves," *The Journal of the Acoustical Society of America,* vol. 120, pp. 1266-1273, 2006.

[43] M. Hong, Z. Su, Y. Lu, H. Sohn, and X. Qing, "Locating fatigue damage using temporal signal features of nonlinear Lamb waves," *Mechanical Systems and Signal Processing,* vol. 60-61, pp. 182-197, 2015.

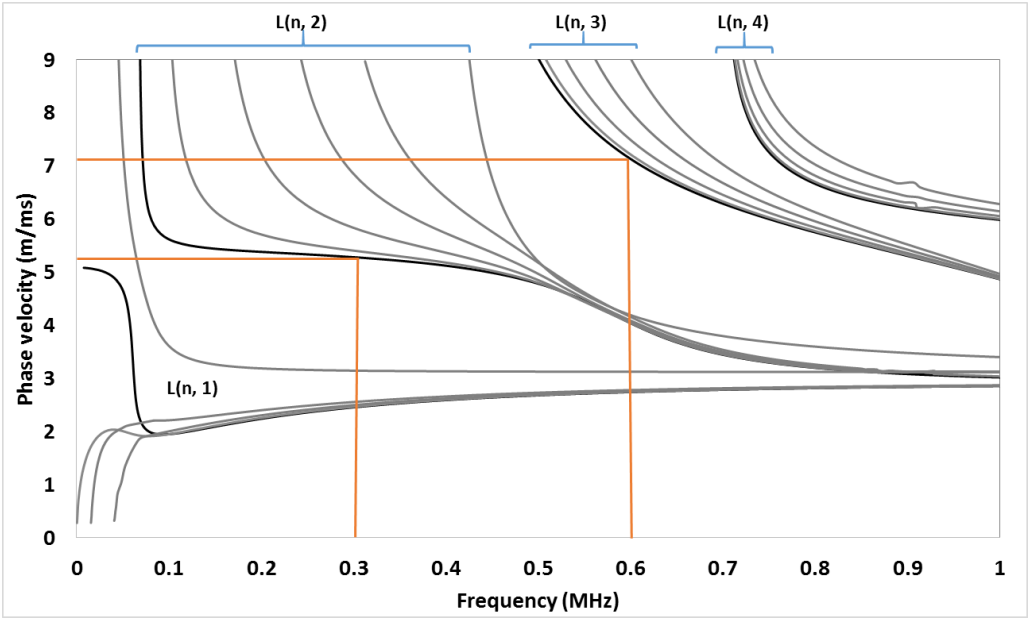

(a)

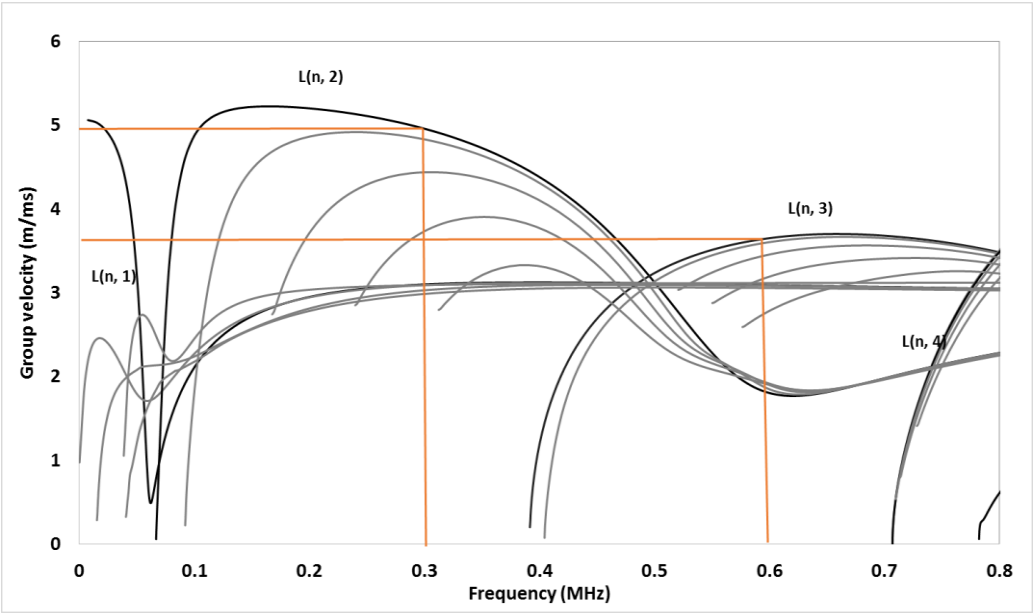

(b)

Figure 1 Dispersion curve of 20 mm diameter and 4 mm wall thickness aluminium pipe. (a) Phase velocity; (b) Group velocity.

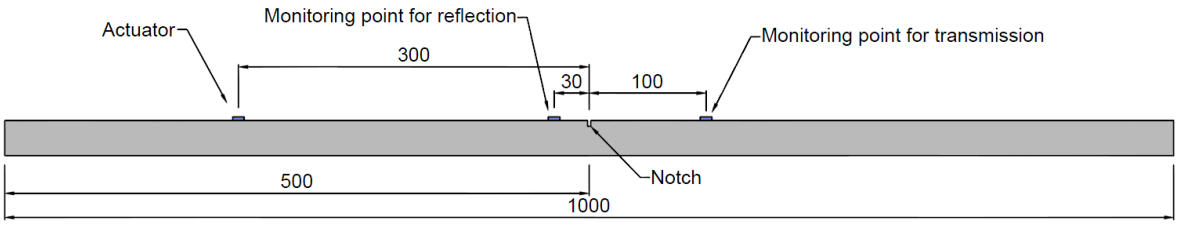

Figure 2 Actuator and sensors arrangement (unit: mm)

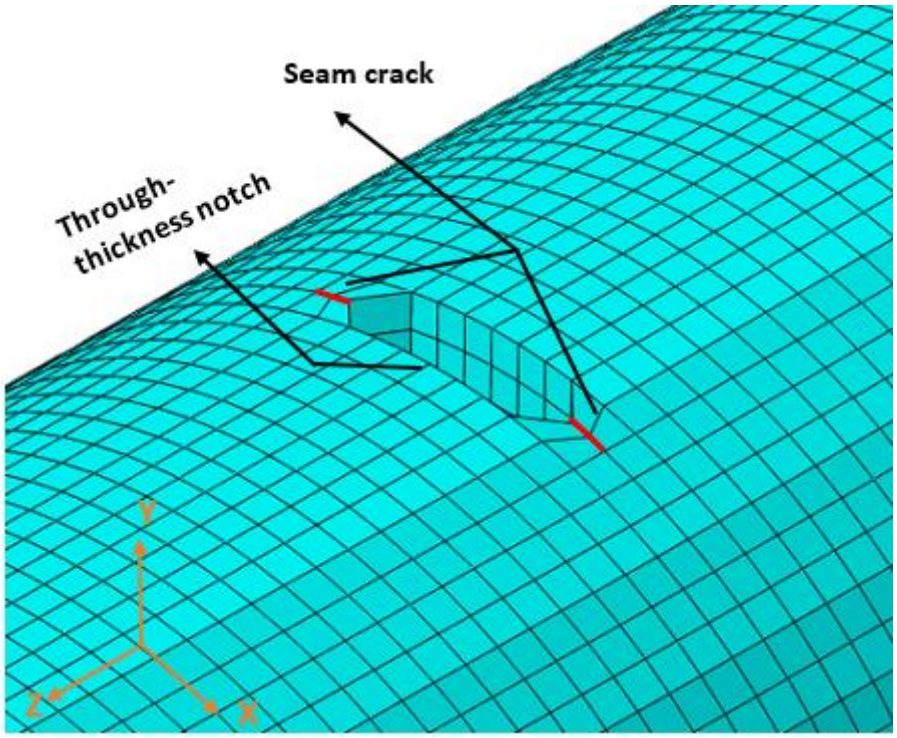

Figure 3 Seam crack in simulation model

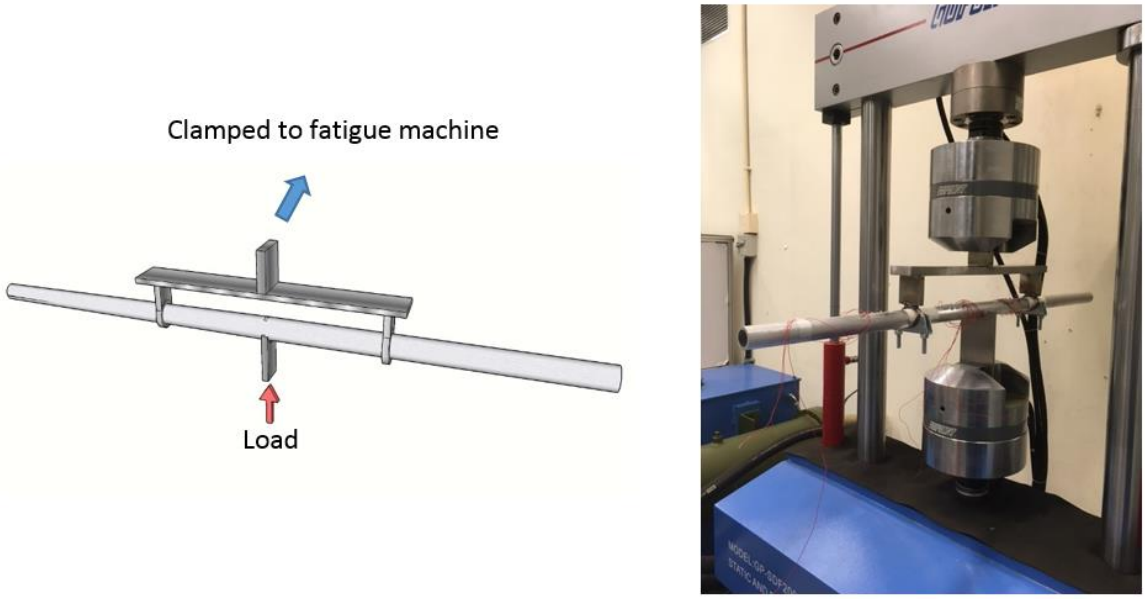

Figure 4 Steel frame combined with fatigue machine for three-point bending fatigue test

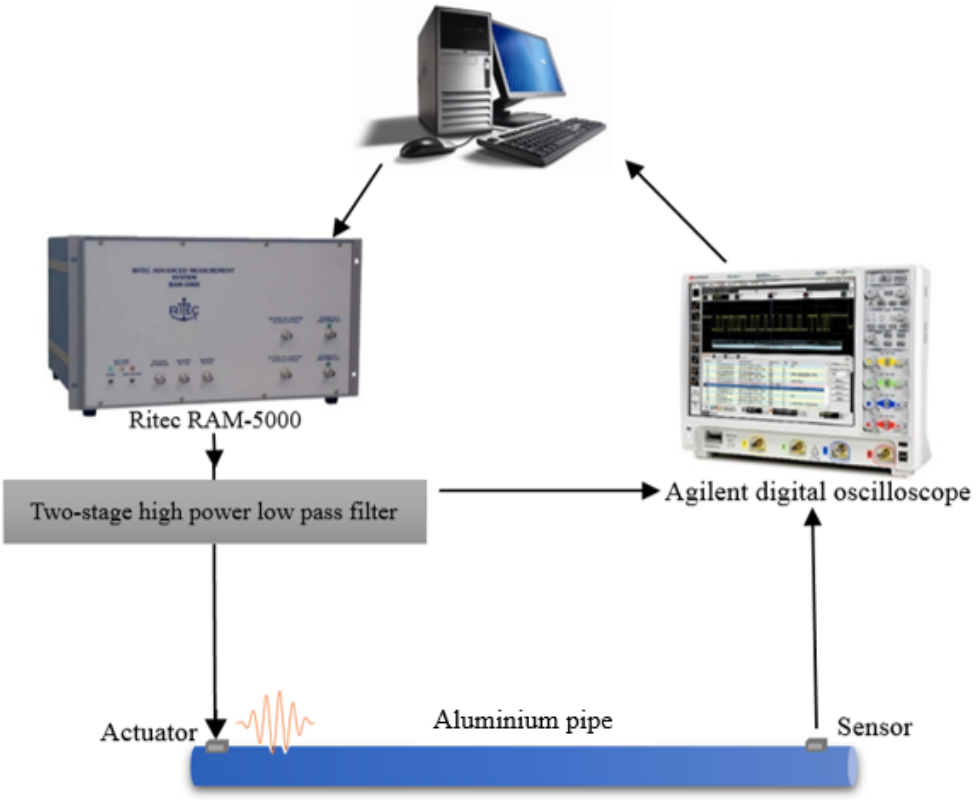

Figure 5 Signal collection system

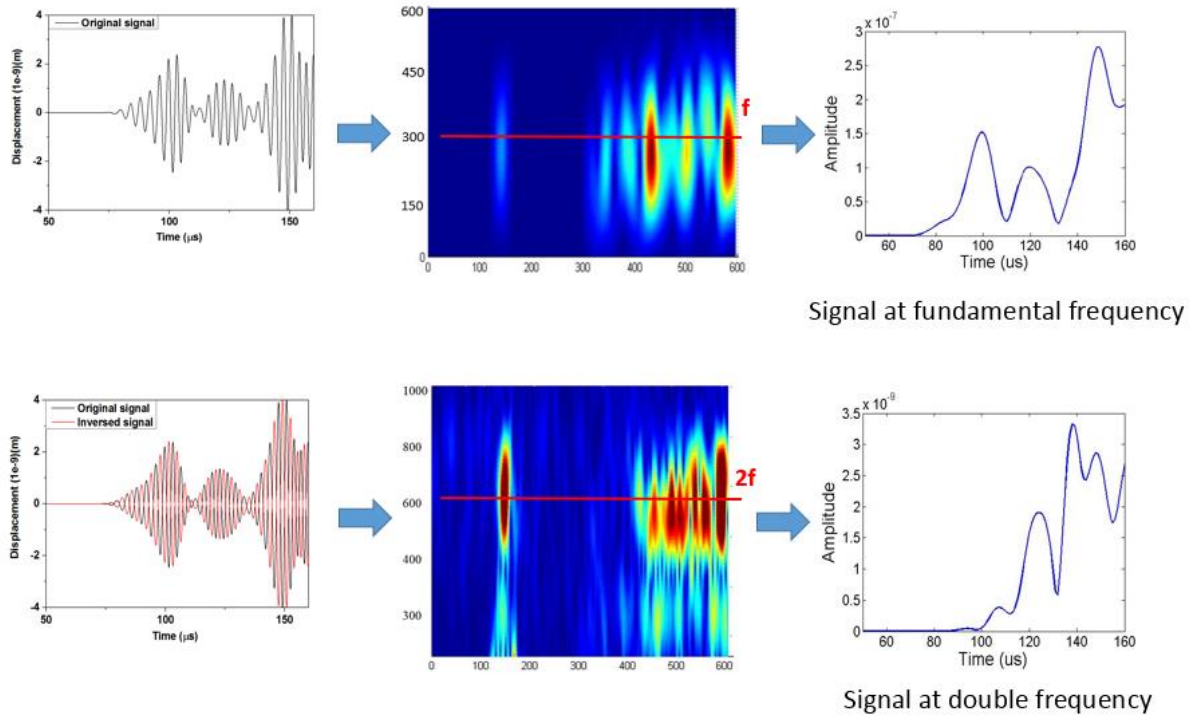

Figure 6 Signal processing procedure

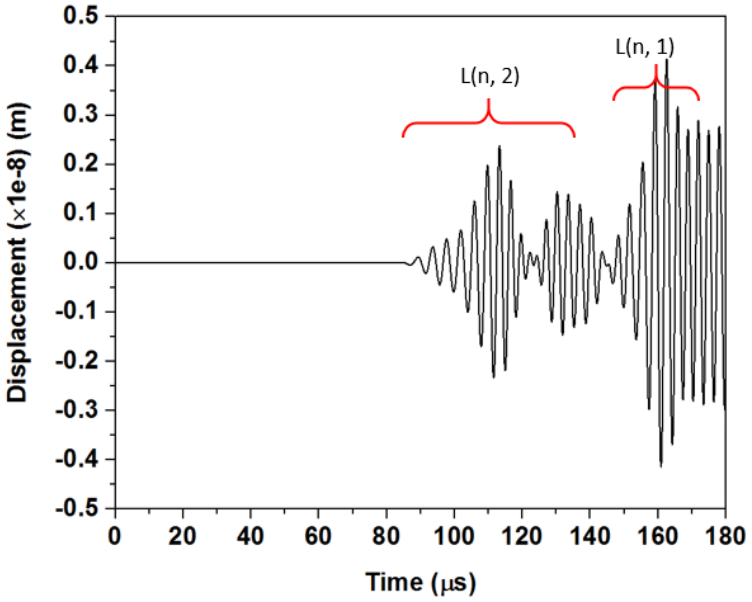

Figure 7 Transmitted signal from simulation model

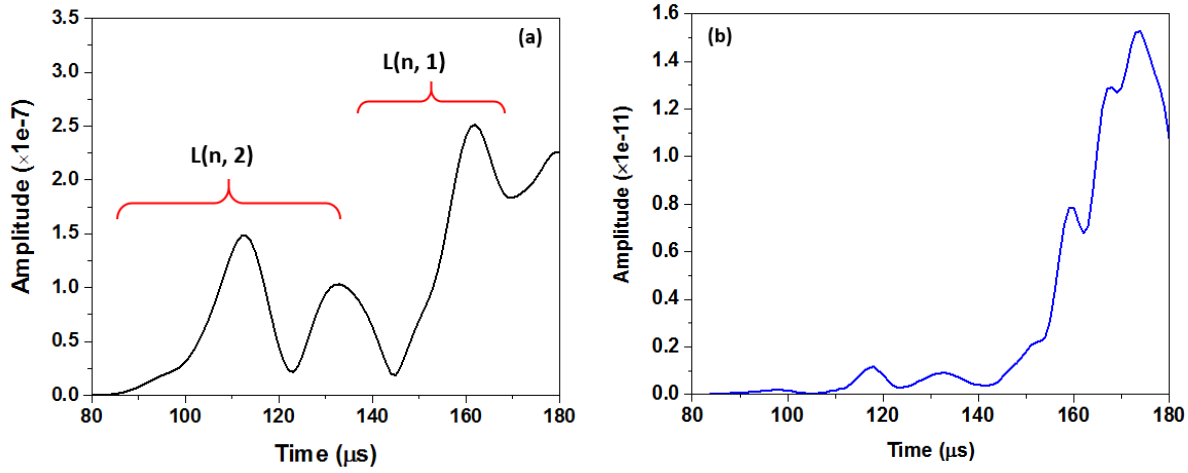

Figure 8 Transmitted signal from model with material nonlinearity after STFT (a) at fundamental frequency; (b) at double frequency.

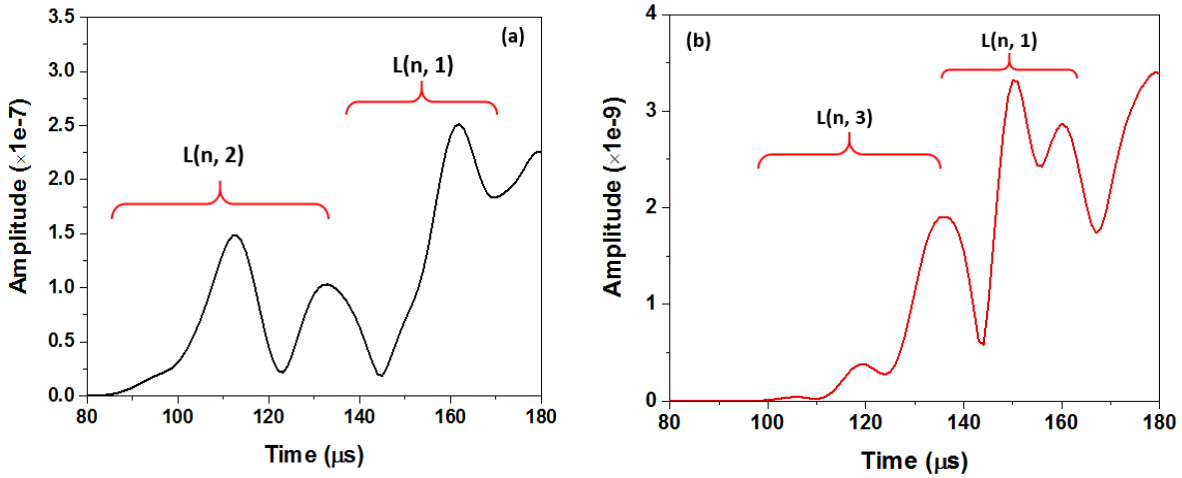

Figure 9 Transmitted signal from model with CAN after STFT (a) at fundamental frequency; (b) at double frequency.

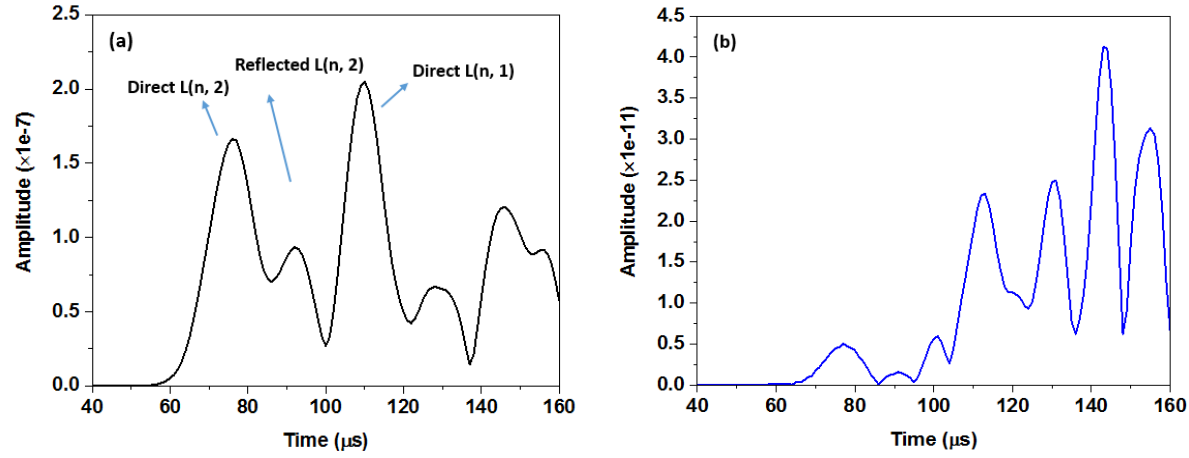

Figure 10 Reflected signal from model with material nonlinearity after STFT (a) at fundamental frequency; (b) at double frequency.

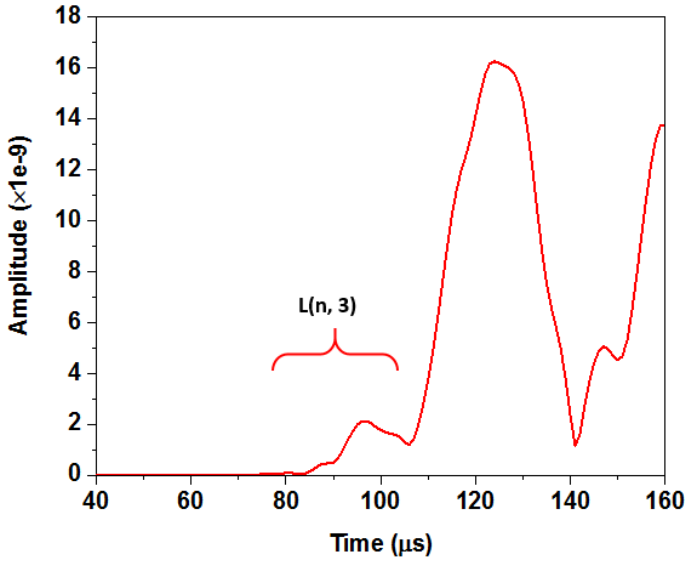

Figure 11 Reflected signal from model with CAN after STFT at double frequency.

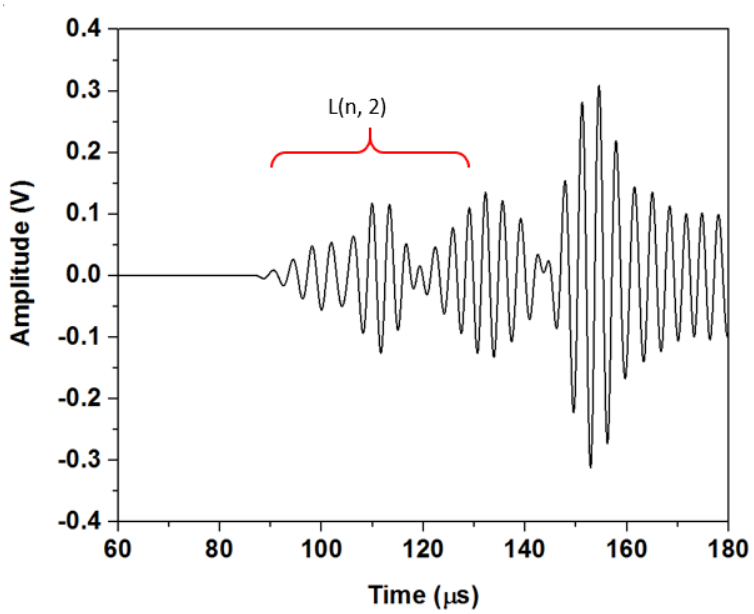

Figure 12 Transmitted signal from experiment

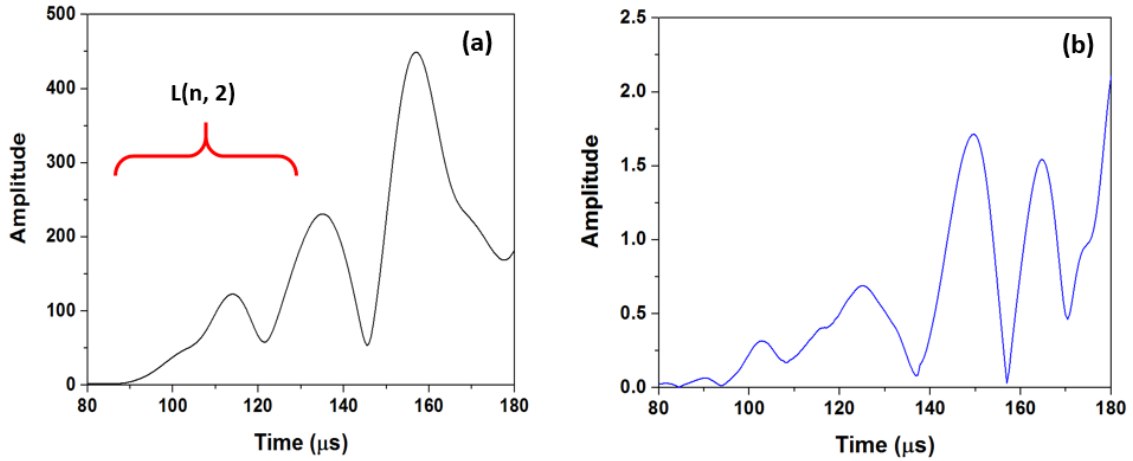

Figure 13 Transmitted signal from experiment before fatigue test after STFT (a) at fundamental frequency; (b) at double frequency.

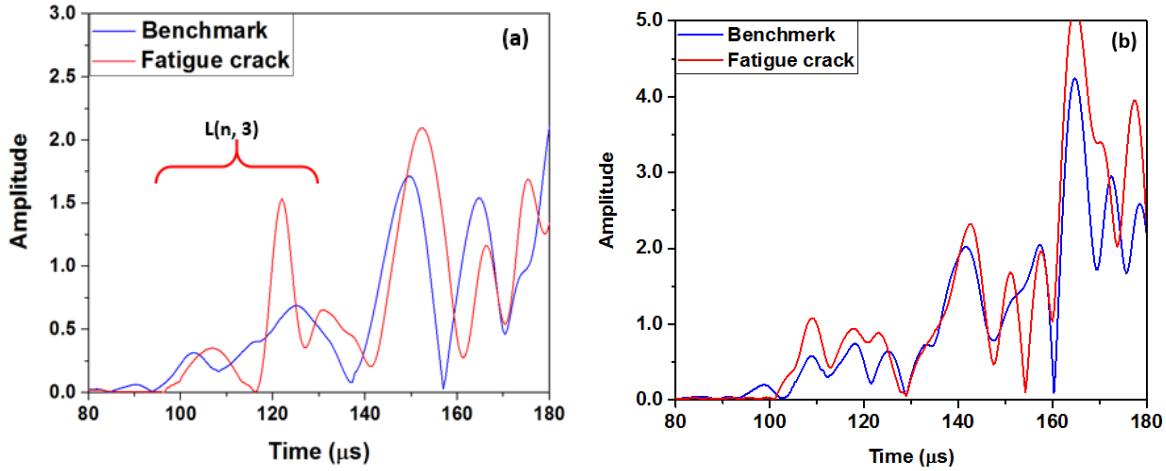

Figure 14 Transmitted signal from experiment before fatigue test (blue line) and after 22000 fatigue cycles (red line) at double frequency (a) specimen 1; (b) specimen 2.

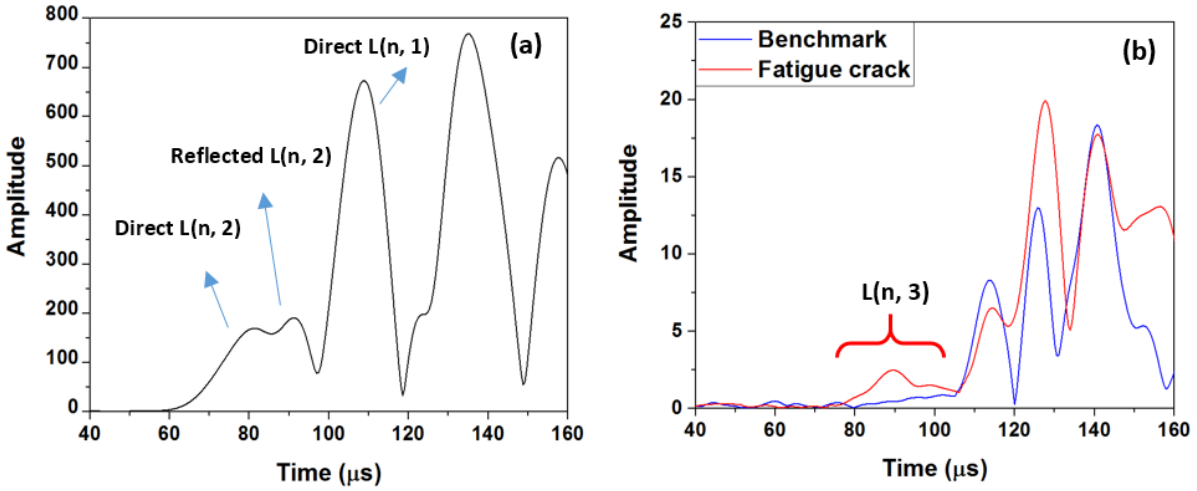

Figure 15 Reflected signal from experiment after 22000 fatigue cycles after STFT (a) at fundamental frequency; (b) at double frequency.

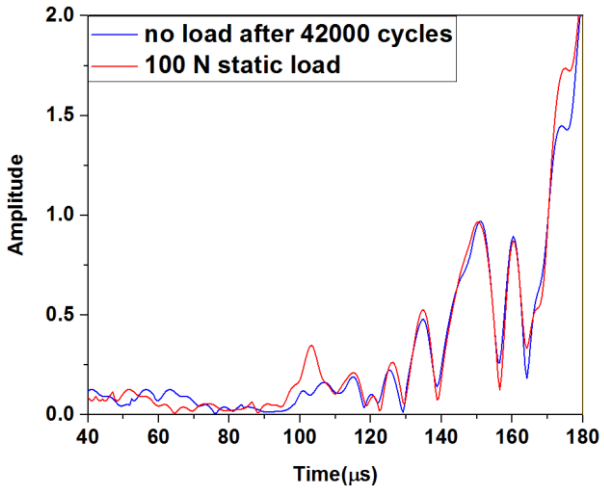

Figure 16 Signals after 42000 fatigue cycles and with static load

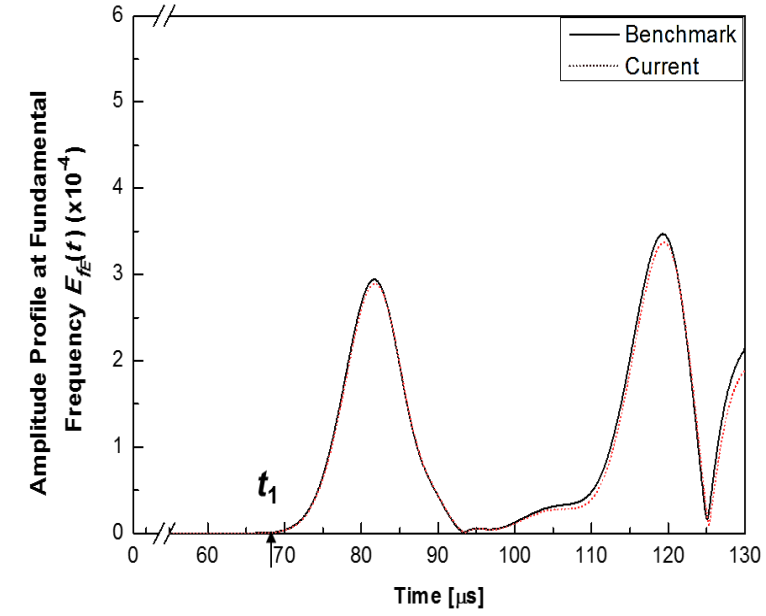

(a)

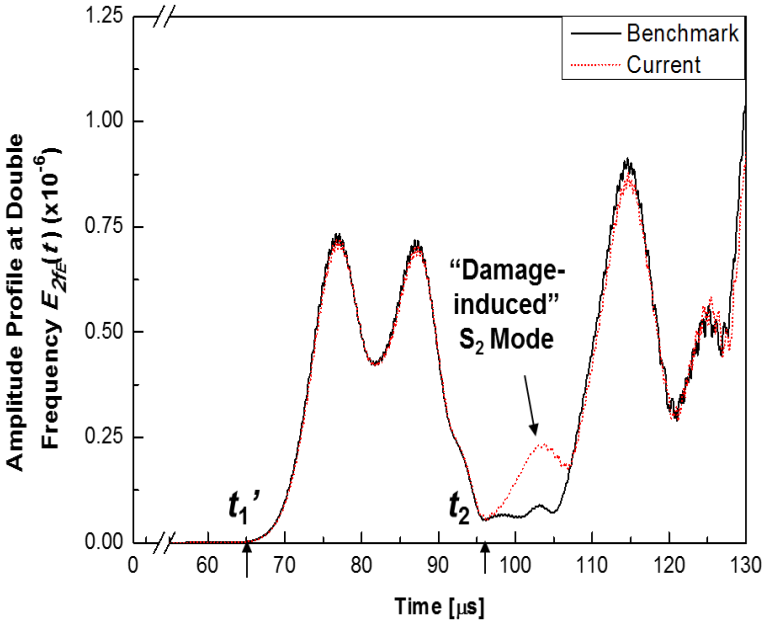

(b)

Figure 17 Transmitted signal from plate specimen in simulation (a) at fundamental frequency; (b) at double frequency [43].

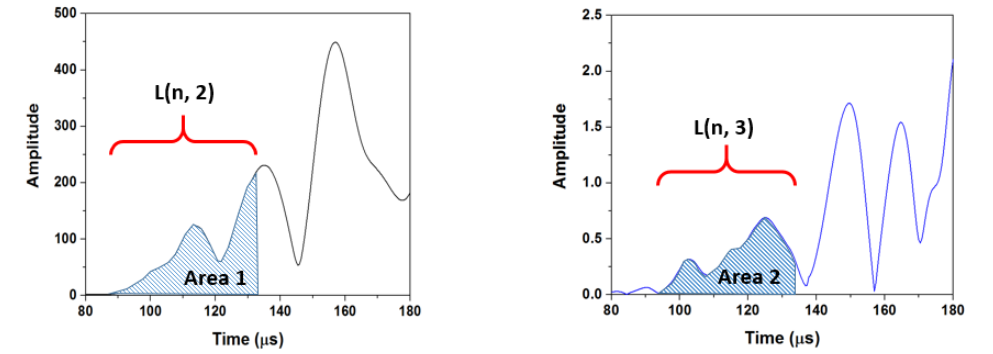

Transmitted signal at fundamental frequency

Transmitted signal at double frequency

$$Nonlinear\ index = \frac{Area\ 2}{Area\ 1}$$

Figure 18 Calculation of nonlinear index

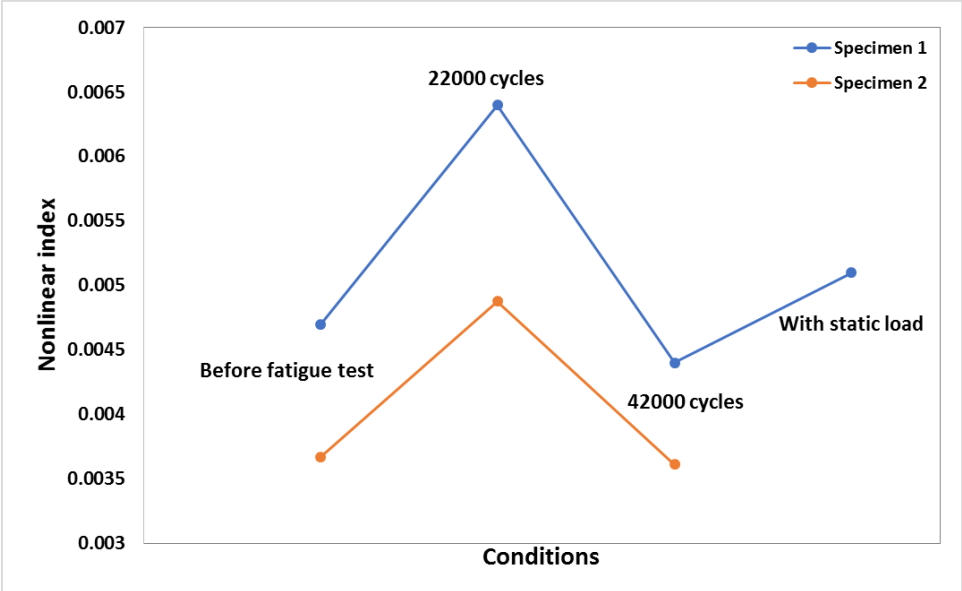

Figure 19 Nonlinear indices under different conditions

Table 1 Material properties for simulation model

Material properties		
Density (kg/m^3)		2700
Young's modulus (GPa)		68.9
Poisson's ratio		0.33
Third order elastic constants (GPa)	A	-320
	B	-200
	C	-190